Journal of Catalysis 350 (2017) 30–40

Contents lists available at ScienceDirect

Journal of Catalysis

journal homepage: www.elsevier.com/locate/jcat

Structure, activity, and selectivity of bimetallic Pd-Fe/SiO_2 and Pd-Fe/γ-Al_2O_3 catalysts for the conversion of furfural

Natalia Pino [a], Surapas Sitthisa [c], Qiaohua Tan [c], Talita Souza [b], Diana López [a], Daniel E. Resasco [c,*]

[a] Química de Recursos Energéticos y Medio Ambiente, Instituto de Química, Facultad de Ciencias Exactas y Naturales, Universidad de Antioquia UdeA, Calle 70 No. 52-21, Medellín, Colombia
[b] University of Minas Gerais, Chemistry Department, Belo Horizonte, MG, Brazil
[c] School of Chemical, Biological and Materials Engineering and Center for Biomass Refining, University of Oklahoma, Norman, OK 73019, USA

ARTICLE INFO

Article history:
Received 2 February 2017
Revised 16 March 2017
Accepted 17 March 2017

Keywords:
Furfural
Furfuryl alcohol
Methylfuran
Pd-Fe alloys
Hydrogenolysis
Hydrogenation
Decarbonylation
Bio-oil upgrading

ABSTRACT

The conversion of furfural has been investigated in vapor and liquid phases over a series of supported monometallic Pd and bimetallic Pd-Fe catalysts. Over the monometallic Pd/SiO_2 catalyst, the decarbonylation reaction dominates, yielding furan as the main product. By contrast, over the bimetallic Pd-Fe/SiO_2 catalyst a high yield of 2-methylfuran is obtained with much lower yield to furan. Interestingly, changing the catalyst support affects the product distribution. For instance, using γ-Al_2O_3 instead of SiO_2 as support of the bimetallic catalyst changed the dominant product from 2-methylfuran to furan. That is, Pd-Fe/γ-Al_2O_3 behaves more like monometallic Pd/SiO_2 than bimetallic Pd-Fe/SiO_2. A detailed characterization of the catalysts via XPS, XRD, and TEM indicated that a Pd-Fe alloy is formed on the SiO_2 support but not on the γ-Al_2O_3 support. Theoretical density functional theory calculations suggest that on the Pd-Fe alloy binding of the furan ring to the surface is weakened compared to on pure Pd. This weakening disfavors the ring hydrogenation and decarbonylation paths, while the oxophilic nature of Fe atoms enhances the interaction of the C=O and the OH groups with the metal surface, which favors the C=O hydrogenation and C—O bond cleavage paths. The presence of the solvent has a less pronounced effect, but clearly has a stronger inhibition on C—C bond cleavage (decarbonylation to furan) than on C—O bond cleavage (hydrogenolysis to methylfuran).

1. Introduction

Furfural (FAL) is a renewable platform molecule derived from lignocellulosic biomass with a good potential to be directly used in the production of fuel components and chemicals [1–3]. Due to its high reactivity, furfural requires selective deoxygenation to obtain compounds stable enough to undergo further upgrading [4]. The selective deoxygenation to 2-methylfuran (MF) is of particular interest since this compound has been proposed as a potential additive to gasoline [5] with good energy density, boiling point, and octane number, as well as a chemical intermediate [6–8]. Therefore, it is important to examine catalysts that effectively break C=O bonds while preserving C—C bonds.

Previous studies [9–11] have shown that Cu-based catalysts are highly selective for furfural hydrogenation to furfuryl alcohol, preserving the C—C bond. Other metals such as Ni and Pd [6,12] catalyze side reactions involving C—C bond scission that consequently reduces the carbon chain length. Bimetallic catalysts [13–17] have attracted attention because they display catalytic properties that differ from those of their parent metals, particularly in the conversion of biomass-derived compounds. As a result, a series of novel catalysts with enhanced selectivity, activity, and stability have been investigated. For example, studies on bimetallic Pd-Cu and Ni-Fe catalysts [7,18] have shown that bimetallic alloys can greatly alter the furfural reaction paths. The incorporation of Cu onto Pd/SiO_2 catalyst, reduced the decarbonylation rate, while increasing the selectivity to hydrogenation products such as furfuryl alcohol. Furthermore, the addition of Fe to silica-supported Ni, changed the product selectivity from furan to 2-methylfuran. This behavior was ascribed to the oxophilic nature of Fe, which makes the di-bonded η^2(C,O)-furfural more stable than on the pure Ni surface and hinders the formation of acyl species, involved in the decarbonylation reaction. In a combined study of density functional theory (DFT) and surface science measurements on Fe/Ni(1 1 1) model surfaces, Yu et al. [19] gave further evidence for the preferential adsorption of furfural via the carbonyl group, with the furan ring tilted away from the surface. In good agreement

* Corresponding author.
E-mail address: resasco@ou.edu (D.E. Resasco).

http://dx.doi.org/10.1016/j.jcat.2017.03.016
0021-9517/

with the conclusions derived from the supported catalyst study [18], these authors concluded that such configuration enhances the production of 2-methylfuran, with furfuryl alcohol acting as an intermediate.

Expanding the investigations of bimetallic catalysts for the conversion of furfural, in this contribution, we have inspected the reaction pathways of furfural over Pd-Fe catalysts. Specifically, we have explored whether different supports may result in varying degrees of metal-metal interaction and consequent modifications of catalytic behavior. To that end, we prepared and characterized bimetallic Pd-Fe catalysts supported on silica (SiO_2) and γ-alumina (γ-Al_2O_3), as two examples of supports that represent weak and strong interaction with the metal components, respectively. To complement and help analyze the experimental results, theoretical density functional theory (DFT) calculations were conducted for Pd and Pd-Fe surfaces. As discussed below, Pd and Fe have been known to produce a range of FCC (face-centered cubic) solid solutions, which depending on composition and temperature can adopt regular FCC, distorted FCC, or even FCT (face-centered tetragonal) structures [20,21]. Our aim in this work was to understand how the formation of the Pd-Fe bimetallic alloy affects the HDO pathway of furfural to produce 2-methylfuran and to determine whether the extent of alloy formation is affected by the support used.

2. Experimental and theoretical methods

2.1. Catalytic materials

Monometallic Pd and bimetallic Pd-Fe catalysts were prepared by incipient wetness impregnation and co-impregnation, respectively, using aqueous solutions of the corresponding metal precursors: $Pd(NO_3)_2{\cdot}6H_2O$ (98%, Alfa Aesar) and $Fe(NO_3)_3{\cdot}9H_2O$ (98% Sigma-Aldrich). The two supports investigated were SiO_2 (PPG Silica Hi-Sil-915) and γ-Al_2O_3 (99.9%, Alfa Aesar). Prior to impregnation, the supports were dried overnight at 120 °C. The Pd loading was kept constant at 1.0 wt% in all preparations, while the Fe loading on the bimetallic Pd-Fe catalysts was 0.5 wt%. After impregnation, the catalysts were first dried overnight at room temperature and then placed in an oven at 120 °C for 12 h. The oven-dried catalysts were finally calcined for 4 h at 500 °C, with a linear heating ramp of 10 °C/min, under 100 ml/min flow of pure air.

The supported Pd and Pd-Fe catalyst samples were reduced in a flow of hydrogen (30 ml/min) at 250 °C and then used in characterization and catalytic activity measurements. For the catalytic activity in gas phase, the catalyst powders were pressed (1500 psi), crushed, and sieved through 40–60 mesh before testing.

2.2. Characterization of the catalysts

Several techniques were employed to characterize the properties and structure of the catalysts. They include N_2 physisorption, X-ray diffraction (XRD), X-ray photoelectron microscopy (XPS) and high-resolution transmission electron microscopy (HRTEM).

The BET surface area (S_g) was measured by conventional N_2 physisorption on a Micromeritics ASAP 2010 unit, after evacuation at 350 °C for 3 h. X-ray diffraction studies were conducted in a Panalytical X'PERT PRO MPD diffractometer with Cu Kα radiation (λ = 1.5406 Å), operated at 45 kV and 40 mA. The data were recorded over 2θ ranges of 30–50° with a step size of 0.026°.

X-ray photoelectron spectroscopy (XPS) analysis was conducted on a Physical Electronics PHI 5800 ESCA system with standard non-monochromatic Al X-rays (1486.6 eV) operated at 250 W and 15 kV in a chamber pumped down to a pressure of approximately 1.0×10^{-8} Torr. A sealed transfer cell was used to transport the ex situ dehydrated samples from a glove box to the analysis chamber without exposure to air. A 93.9 eV and 58.7 eV pass energy was typically used for survey and specific element analysis, respectively. The electron take-off angle was 45° with respect to the sample surface. The binding energies were adjusted to the C signal at 284.6 eV as an internal reference.

Morphology and particle size of the Pd/SiO_2, $Pd\text{-}Fe/SiO_2$ and $Pd\text{-}Fe/\gamma\text{-}Al_2O_3$ catalysts were characterized by transmission electron microscopy (TEM – Tecnai F20 Super Twin TMP), with a resolution of 0.1 nm, at 200 kV accelerating voltage. Prior to the analysis, the samples were reduced ex situ in flowing H_2 at 250 °C for 3 h. The reduced samples were suspended in propanol by sonication, deposited on a TEM (Cu) grid, and dried overnight. The particle size and crystallographic planes were measured from HRTEM images using DigitalMicrograph and ImageJ software.

2.3. Catalytic activity

The furfural conversion over Pd and Pd-Fe catalysts was evaluated in liquid and vapor phase, with the purpose of investigating how the reaction medium affects the mechanism and product distribution.

2.3.1. Vapor phase

The vapor-phase conversion of furfural over $1\%Pd/SiO_2$, $1\%Pd\text{-}0.5\%Fe/SiO_2$ and $1\%Pd\text{-}0.5\%Fe/\gamma\text{-}Al_2O_3$ catalysts was studied in a 1/4″ tubular quartz reactor. The pelletized catalyst (size range: 250–425 μm) was placed at the center of the reactor between two layers of glass beads and quartz wool. Calculations were done to ensure that external and internal mass transfer limitations were eliminated following the criteria proposed by Madon and Boudart [22]. The catalyst was pre-reduced in flow of H_2 (60 ml/min, Airgas, 99.99%) for 1 h at 250 °C. After reduction, the catalyst was cooled down to the selected temperature (210–250 °C) under the same H_2 flow rate. Prior to the reaction, the as-received furfural (Sigma-Aldrich, 99.5%, brown color) was purified by vacuum distillation to remove residues and any oligomers formed during storage. The purified liquid was kept under He atmosphere until its use in the reaction test. This is an important step to minimize deactivation by deposition of oligomers over the surface.

A 0.5 ml/h flow of liquid furfural was fed continuously from a syringe pump (Cole Palmer) and vaporized into a gas stream of 60 ml/min H_2. To keep all the compounds in the vapor phase all lines before and after the reactor were kept heated at 220 °C using heating tapes. To vary the space time (W/F = catalyst mass/mass flow rate of reactant), the amount of catalyst was varied in the range 0.02–0.15 g. Catalysts were mixed with glass bead when loading and the catalyst bed L/D ratio is about 5. The reaction products were analyzed online on a gas chromatograph (Agilent model 6890) using an HP-5 capillary column (30 m/0.25 mm/0.25 μm) and a FID detector.

The product yield and selectivity for each product were calculated as follows:

$$Yield\ (\%) = \frac{moles\ of\ product}{moles\ of\ furfural\ fed} \times 100 (1) \quad (1)$$

$$Selectivity\ (\%) = \frac{moles\ of\ product}{moles\ of\ furfural\ consumed} \times 100 \quad (2)$$

2.3.2. Liquid phase

The liquid phase conversion of furfural was investigated in a 50 ml Parr Reactor using decahydronaphthalene (decalin, *cis* + *trans* mixture, 98% purity, Sigma-Aldrich) as a solvent. For the catalytic reaction runs, 20 ml of decalin, 0.5 ml of furfural and

20 mg of catalysts (1%Pd/SiO_2, 1%Pd-0.5%Fe/SiO_2 and 1%Pd-0.5%Fe/γ-Al_2O_3) were added into the reactor vessel. The liquid phase experiments were performed under H_2 at 4 MPa and 250 °C. To minimize the effect of catalyst deactivation, the reaction time was kept at 1 h for all the runs with a stirring speed of 400 rpm.

At the end of each run, the products were separated from the catalyst by centrifugation and filtration. The liquid products were identified and quantified by gas chromatography. A Shimadzu QP2010 GC–MS equipped with a mid-polarity (Phenomenex ZB-1701) capillary column, 60.0 m × 0.25 mm × 0.25 μm nominal, was used for product identification, while a GC-FID Agilent 7890B was used for quantitative analysis. In all the GC-FID analyses, phenol was used as internal standard to help close the mass balances. The product yield and selectivity for each product were calculated using Eq. (1) and Eq. (2), respectively.

2.4. Density functional theory (DFT) calculations

All DFT calculations were performed with the Vienna ab initio simulation package (VASP) [23]. The GGA-PBE functional [24], all-electron plane-wave basis sets with an energy cutoff of 400 eV, and a projector augmented wave (PAW) [25] method were adopted. A Brillouin-zone of p(4 × 4) lateral supercell was sampled by 3 × 3 × 1 k-points using the Monkhorst–Pack scheme. The convergence threshold was set to 10^{-6} eV in total energy and 10^{-2} eV/Å in force on each atom.

It was reported that both Pd and Fe in the PdFe/SiO_2 catalyst can be reduced to their metallic state (zero valence) at the temperature as low as 400 K, and the main Pd-Fe alloy phases are PdFe and Pd_3-Fe [26–29]. Thus the two Pd_3-Fe_1 and Pd_2-Fe_2 crystal structures, shown in Fig. 1 along with those of pure Pd, were used to model the Pd-Fe alloy herein. Their structures were optimized and the lattice constants were calculated with $a = b = c = 3.94$ Å for the Pd, $a = b = c = 3.88$ Å for the Pd_3-Fe_1 alloy and $a = b = 3.83$ Å & $c = 3.78$ Å for the Pd_2-Fe_2 alloy, which were close to the lattice constants measured by experiments [30]. The closed packed 4 × 4 Pd (1 1 1), Pd_3-Fe_1(1 1 1) and Pd_2-Fe_2(1 1 1) surfaces were modeled by a four-layer slab with the bottom two layers fixed in their bulk positions while the top layers were allowed to relax. The two successive slabs were separated by a 15 Å vacuum region to ensure that the adsorbate (e.g., furfural, furfuryl alcohol) and the subsequent slab would not interact.

The adsorption energy (E_{ads}) in this work is defined as $E_{ads} = E_{adsorbate/surf} - E_{surf} - E_{adsorbate}$, where $E_{adsorbate/surf}$, E_{surf}, and $E_{adsorbate}$ are the total energy of the adsorbate on the surface, the clean surface, and the gas-phase adsorbate in vacuum.

The core-level shifts of Pd_{3d} in the bulk Pd_3Fe_1 and Pd_2Fe_2 crystals compared to Pd were calculated in reference to the Fermi energy using the final state approximation [31,32].

3. Results and discussion

3.1. Catalyst characterization

3.1.1. BET surface area

The BET surface areas were measured by N_2 physisorption. In line with the surface areas reported by the manufacturers, the silica support exhibited a higher surface area (130 m^2/g) than γ-alumina (90 m^2/g). No significant drops in surface area were observed after impregnation of the metals and thermal treatment.

3.1.2. X-ray diffraction

XRD patterns of the mono and bimetallic samples were obtained on pre-reduced samples. Fig. 2 compares the diffractograms of Pd-Fe on the two supports to those of Pd/SiO_2. The characteristic diffraction peaks at $2\theta = 40.1°$ and 46.8° corresponding to Pd(1 1 1) and (2 0 0) crystal faces are clearly observed in the XRD pattern of Pd/SiO_2. Remarkably, these peaks do not appear in the XRD pattern of the Pd-Fe/SiO_2 catalyst, but rather two new peaks are observed at around 41.2 and 47.2°, which can be ascribed to the formation of a Pd-Fe alloy when the SiO_2 support is used. Since Fe atoms are smaller than Pd atoms, when incorporated in the Pd FCC structure, they cause a shift of the 2θ diffraction angles to larger values, as observed here for the Pd-Fe/SiO_2 catalyst and in previous studies on analogous Pd-Fe bimetallic catalysts [33,34]. This is also in agreement with our DFT calculations that the lattice constants for the Pd-Fe alloys Pd_3Fe_1 (3.88 Å) and Pd_2Fe_2 (3.83 Å) are smaller than the pure Pd (3.94 Å). There is a linear decrease in the unit cell edge with the incorporation of iron. By contrast, no evidence of crystalline Pd or Pd-Fe alloys was seen in the XRD pattern of the Pd-Fe/γ -Al_2O_3 catalyst. Only the peaks associated with γ-Al_2O_3 [35] were detectable in this sample. This could be due to a higher dispersion of Pd on this type of support.

In the Pd-Fe/SiO_2 catalyst, the diffraction peaks became much weaker compared to those in the pattern of the monometallic Pd catalyst, which indicate the better dispersion of Pd particles with the introduction of Fe by the formation of Pd-Fe alloys and show the advantages of a bimetallic catalyst over a monometallic catalyst in the dispersion of the metal sites.

3.1.3. X-ray photoelectron spectroscopy (XPS)

XPS was used to verify the formation of a binary alloy in the bimetallic catalyst. For this purpose, binding energies for the Pd-Fe catalyst were compared to those of pure Pd. For instance, the XPS spectra for the ex situ reduced (transferred avoiding exposure to air) Pd and Pd-Fe catalysts are shown in Fig. 3.

The binding energies observed on the Pd/SiO_2 catalyst of 335.4 and 340.8 eV can be definitely assigned to Pd $3d_{5/2}$ and $3d_{3/2}$ of metallic palladium [36–38]. In comparison, a clear shift of 0.4 eV

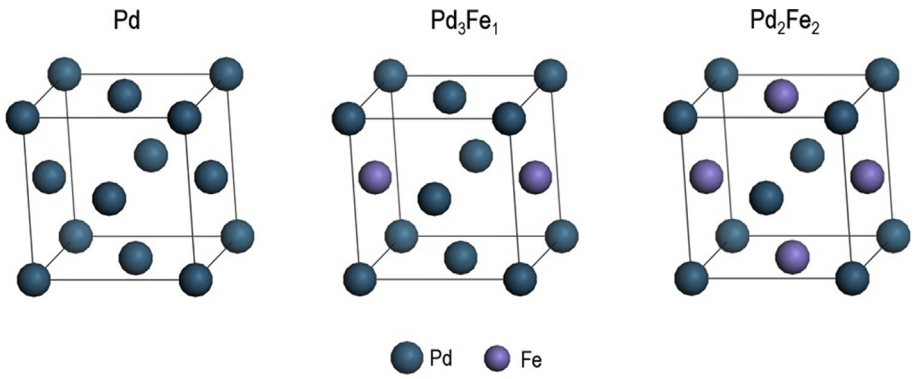

Fig. 1. Bulk monometallic Pd and bimetallic Pd-Fe alloy structures. Blue and purple spheres represent Pd and Fe, respectively.

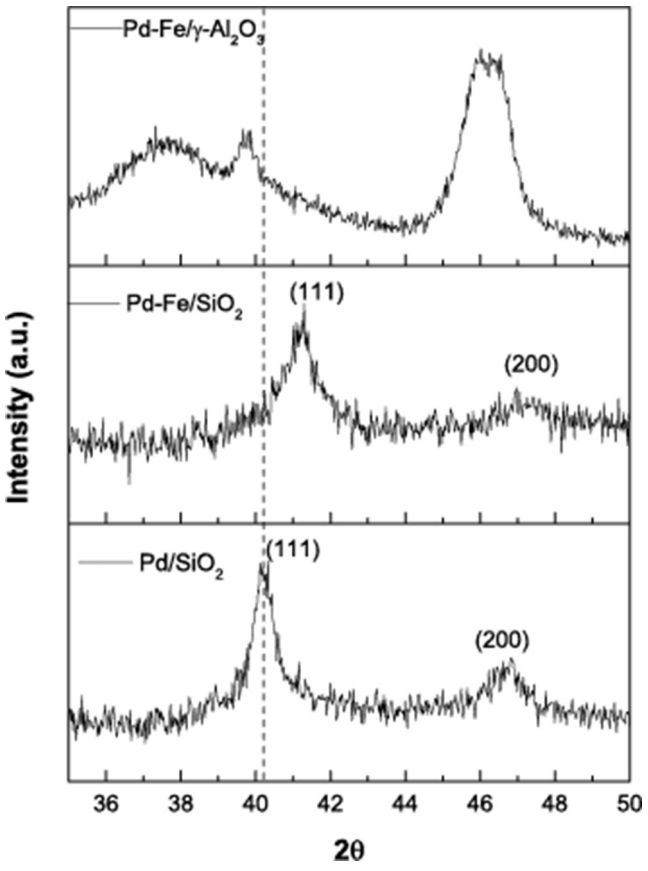

Fig. 2. XRD patterns of the samples after reduction. The (111) and (200) peaks of the fcc crystal structure (Pd or Pd-Fe alloy) are indicated.

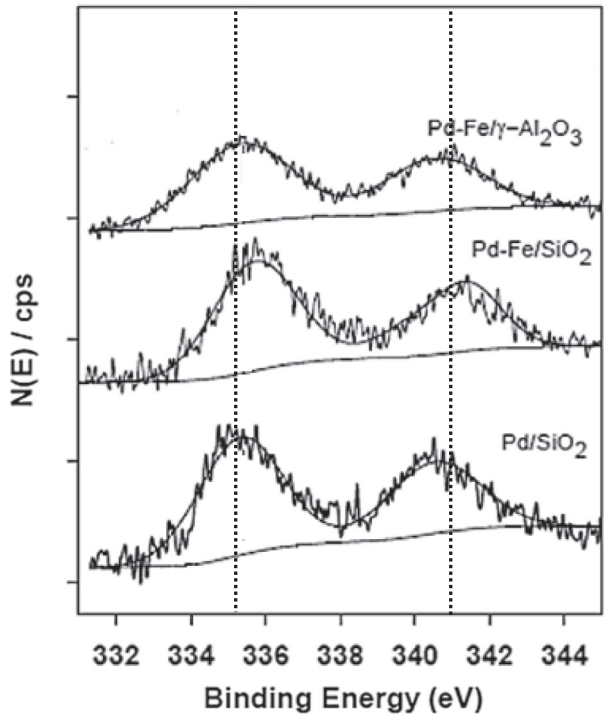

Fig. 3. X-ray photoelectron spectroscopy (XPS) of Pd_{3d} for Pd and Pd-Fe catalysts with different supports.

to higher binding energies is reproducibly observed for the Pd-Fe/SiO_2 catalyst. This shift has been previously detected when Pd-Fe alloys are formed. For example, Tang et al. [34] observed a positive binding energy shift in Pd-Fe/C samples compared to a Pd/C sample. Similarly, Felicissimo et al. [39] observed shifts to higher binding energies when Fe was deposited on top of Pd. As the amount of Fe increased, the binding energy for Pd 3d continuously shifted up to 0.6 eV above the value of pure Pd, while the intensity decreased, as expected. The Fe 2p spectra showed an inverse trend, with a continuous shift to lower binding energies. The same trend has been reported by other authors [40,41], who have consistently observed a positive shift with respect to the pure Pd when the Pd-Fe alloy is formed. Therefore, based on previous observations, it is reasonable to conclude that the observed binding energy shift for Pd-Fe/SiO_2 (Fig. 3) can be taken as an evidence of alloy formation.

While we can take the binding energy shift as an indication of Pd-Fe alloy formation, the fundamental cause for this shift may be a matter of debate. Some authors have concluded that the concomitant shifts in binding energies, that is Pd up and Fe down, reflect an electron transfer from Pd to Fe, which would be the opposite to that predicted by simple analysis of electronegativities of the two metals (Pd:2.2 and Fe:1.83).

Felicissimo et al. [39] have cautioned that binding energy shifts may not only contain contributions of initial state effects, such as electron transfer, but also orbital rehybridization and final state effects. This is further confirmed by our DFT calculations of the Pd_{3d} core-level shift in the monometallic Pd and bimetallic Pd-Fe alloy bulk structures (Table 1), which clearly show that alloying Pd with Fe leads to the Pd_{3d} core-level shift of 0.35 eV in the Pd_3Fe_1 alloy and 0.52 eV in the Pd_2Fe_2 eV.

Contrary to the XPS spectrum of the Pd-Fe/SiO_2 catalyst that clearly shows the presence of a Pd-Fe alloy, the Pd-Fe/γ-Al_2O_3 spectrum shows no shift in binding energy compared to that of Pd/SiO_2, which would indicate that Pd on alumina is not affected by the presence of Fe. That is, while formation of Pd-Fe alloys is favorable on the SiO_2 support it is much less so on γ-Al_2O_3. In a study of bimetallic Rh-Au catalysts supported on silica or alumina, Nunez and Rouco [42] observed similar differences in the extent of metal-metal interaction between the two supports, as those reported here. Specifically, they observed that the hydrogenolysis activity and the reducibility (TPR) of the bimetallic catalyst supported on γ-Al_2O_3 could be considered as a simple sum of the independent monometallic catalysts. By contrast, both the activity and reducibility (TPR) of the bimetallic catalysts supported on SiO_2 clearly gave evidence of the formation of a bimetallic cluster, showing a significant drop in activity and a single reduction peak in TPR. That is, a weak interacting support such as SiO_2 allows high enough mobility to the metal precursors to intermingle efficiently and form a metallic alloy upon reduction. Indeed, this conclusion is in good agreement with the differences in the product distribution described in the next section.

TEM analysis was conducted on pre-reduced samples to obtain information on the size and microstructure of the metal particles. Fig. 4 shows the micrographs and corresponding particle size distribution histograms of Pd/SiO_2, Pd-Fe/SiO_2 and Pd-Fe/γ-Al_2O_3 samples. It is interesting to note the effect of the support on the metal dispersion. With the Pd-Fe/γ-Al_2O_3 catalyst, the distribution of metal particles is more homogeneous, with an average size smaller than on the other samples. It appears that the metal interaction with alumina is higher than on silica, which is consistent with XRD results and the discussion above. Specifically, the average particle sizes, estimated by random measurement of 50 nanoparticles from the corresponding TEM images, were 6.9 ± 1.7 nm, 4.1 ± 0.8 nm, 2.5 ± 0.8 nm for Pd/SiO_2, Pd-Fe/SiO_2, Pd-Fe/γAl_2O_3, respectively. Comparing Pd/SiO_2 and Pd-Fe/SiO_2

Table 1
Comparison of XPS measured Pd_{3d} binding energies in Pd/SiO_2 and $Pd\text{-}Fe/SiO_2$ and the DFT calculated core-level binding energy of Pd_{3d} in Pd (fcc) and Pd-Fe (fct) bulk structures.

XPS	Pd/SiO_2	$Pd\text{-}Fe/SiO_2$		Shift	
	335.4	335.8 eV		+0.4 eV	
DFT	Pd (fcc)	Pd_3Fe_1	Pd_2Fe_2	Pd_3Fe_1	Pd_2Fe_2
	–	–	–	+0.35 eV	+0.52 eV

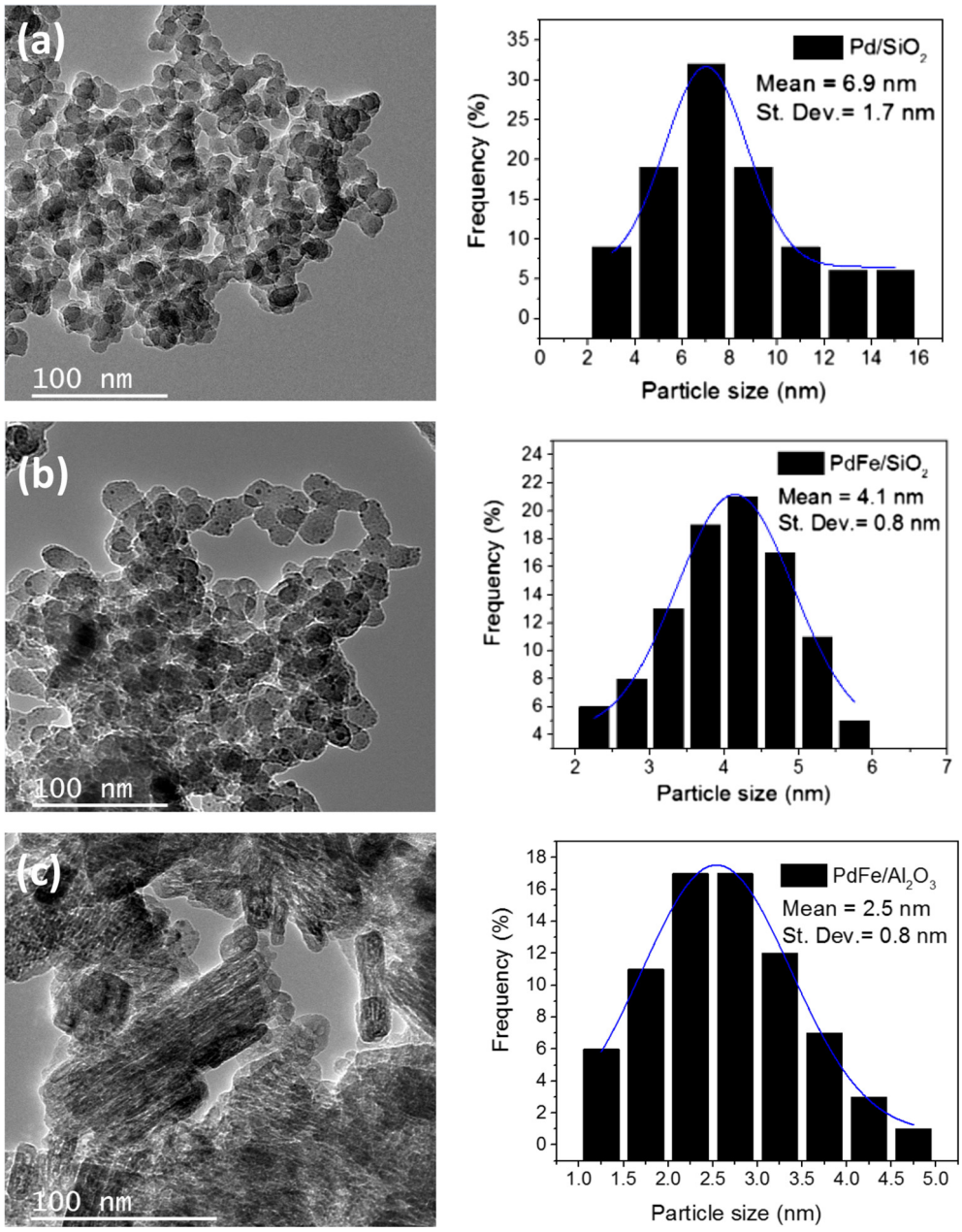

Fig. 4. TEM images of (a) Pd/SiO_2, (b) $Pd\text{-}Fe/SiO_2$, and (c) $Pd\text{-}Fe/\gamma\text{-}Al_2O_3$ catalysts with the corresponding particle size distribution histograms.

catalysts, it can be observed that the Pd-Fe alloy nanoparticles on the silica support are noticeably smaller and more uniform in size than those on the monometallic Pd/SiO_2 sample. The introduction of Fe reduced the aggregation of Pd particles significantly during the preparation procedure, which resulted in a better dispersion and smaller sizes of the metal particles. It seems that the interaction between the two metals has a stabilizing effect that results in inhibition of metal sintering.

Additional HRTEM and STEM-EDX data are included in the Supplemental Information for the $Pd\text{-}Fe/SiO_2$ and $Pd\text{-}Fe/\gamma Al_2O_3$ samples. They give further evidence that on the silica support, Pd-Fe alloy particles are obtained, but on the alumina-supported bimetallic catalyst, the two metals are segregated.

3.2. Catalytic activity

3.2.1. Vapor phase conversion of furfural over Pd/SiO_2 and $Pd\text{-}Fe/SiO_2$

The product distribution obtained over the Pd/SiO_2 catalyst at 250 °C is shown in Fig. 5. In agreement with our previous study of furfural conversion over pure Pd catalysts [43], the main product

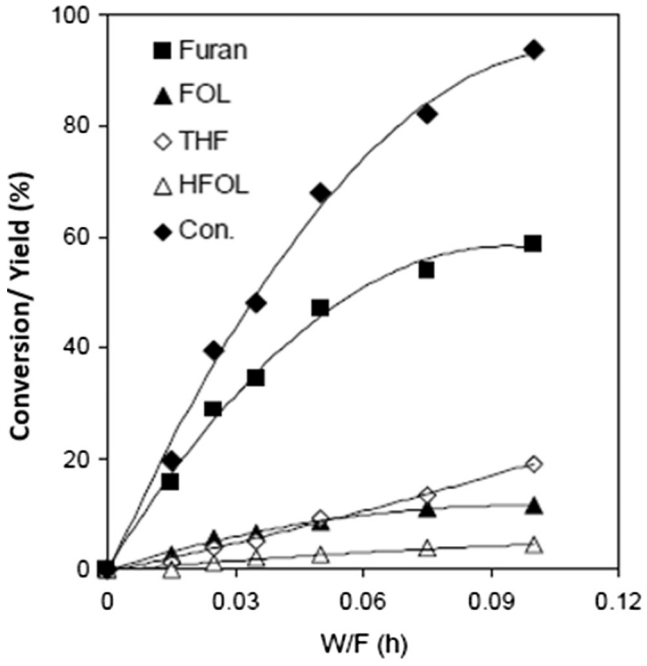

Fig. 5. Product distribution from the reaction of furfural over a monometallic 1%Pd/SiO_2 catalyst, at 250 °C, H_2/Feed molar ratio = 25, pressure = 1 atm. FOL = furfuryl alcohol, THF = tetrahydrofuran, HFOL = tetrahydrofurfuryl alcohol.

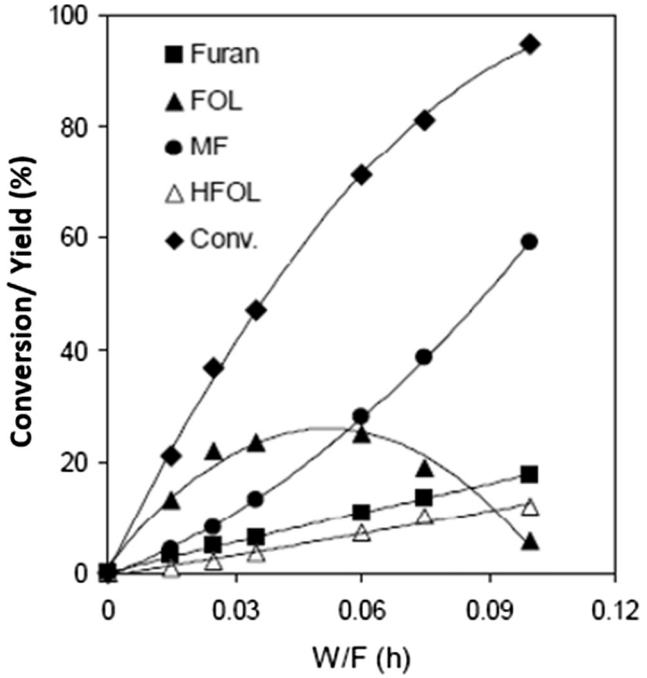

Fig. 6. Product distribution from the reaction of furfural over a bimetallic 1%Pd-0.5%Fe/SiO_2 catalyst, at 250 °C, H_2/Feed molar ratio = 25, pressure = 1 atm. FOL = furfuryl alcohol, MF = 2-methylfruan, HFOL = tetrahydrofurfuryl alcohol.

from the reaction of furfural on 1%Pd/SiO_2 at 250 °C is furan, from direct decarbonylation [44]. At the same time, hydrogenation of furfural to furfuryl alcohol was also observed, but to a much lesser extent than decarbonylation (~10% vs. 60% yield at W/F = 0.1 h). In fact, furfuryl alcohol is the dominant product over Cu, on which the metal-carbon bond strength is very weak [39–46]. The secondary ring hydrogenation of the primary products (furan and furfuryl alcohol) to tetrahydrofuran and tetrahydrofurfuryl alcohol (HFOL), respectively, was only observed at higher W/F.

It must be noted that, regardless of the conversion level, no 2-methylfuran was formed. That is, pure Pd does not exhibit a high catalytic activity for C—O bond cleavage, but the high selectivity toward furan, accompanied by an equimolar production of carbon monoxide, indicates that Pd is highly selective for decarbonylation, as previously shown [39,40].

As shown in Fig. 6, interesting differences in product distribution were observed when Fe was incorporated into the Pd/SiO_2 catalyst. A remarkable change in product selectivity is observed over 1%Pd-0.5%Fe/SiO_2 catalyst compared to the pure Pd catalyst. It is clear that the main products from the reaction of furfural over 1%Pd-0.5%Fe/SiO_2 catalyst are furfuryl alcohol and, notably, 2-methylfuran, which is not observed over 1%Pd/SiO_2.

From the evolution of product distribution as a function of W/F, it can be seen that 2-methylfuran is in fact a secondary product derived from the hydrogenolysis of the C—O bond in furfuryl alcohol, rather than directly from furfural. That is, the yield of furfuryl alcohol is dominant at low W/F and increases with increasing W/F, reaching a maximum and then decreases. Simultaneously, the production of 2-methyl furan starts with a very low slope at W/F = 0, but gradually increases with W/F. The secondary product nature of 2-methyl furan is further demonstrated in Table 2, which summarizes the conversion and product distribution obtained from the reaction of furfural (FAL) and furfuryl alcohol (FOL) over the Pd/SiO_2 and Pd-Fe/SiO_2 catalysts. A much higher yield of 2-methylfuran was observed when furfuryl alcohol was used as a feed over Pd-Fe/SiO_2 instead of furfural (compare entries 2 vs. 6).

Also, a comparison of product distributions at the same furfural conversion and temperature is made in entries 1 and 2 for 1%Pd/SiO_2 and 1%Pd-0.5%Fe/SiO_2 catalysts, respectively. The yield of furan derived from decarbonylation is dramatically decreased on Pd-Fe/SiO_2 (13.5%) compared to 54% on Pd/SiO_2. Furthermore, contrary to monometallic Pd catalyst that does not form any 2-methylfuran, the 1%Pd-0.5%Fe/SiO_2 catalyst produced 2-methylfuran in significant amounts, particularly at high W/F. To show that the enhanced rate of 2-methylfuran production on the Pd-Fe bimetallic catalyst prepared by co-impregnation technique is due to a direct interaction between Pd and Fe, a physical mixture of monometallic 1%Pd/SiO_2 and 1%Fe/SiO_2 (entry 3) was tested and compared in the table. The results show that the product distributions and furfural conversions from 1%Pd/SiO_2 and a physical mixture of 1%Pd/SiO_2 and 1%Fe/SiO_2 are essentially the same. That is, furan from decarbonylation of furfural is the main product while 2-methylfuran is not formed. It should be noted that under the present conditions, the monometallic Fe/SiO_2 exhibits no activity for the reaction of furfural and furfuryl alcohol (entries 4 and 8).

It is clear that the presence of Fe on bimetallic catalyst has both a promoting effect and a suppressing effect on a product yield and selectivity. The yield of furfuryl alcohol from hydrogenation of furfural and 2-methylfuran from hydrogenolysis of furfuryl alcohol is promoted while the yield of furan from decarbonylation is suppressed. This will be further illustrated by DFT calculations below.

The similar behavior was also observed when having furfuryl alcohol as feed over Pd/SiO_2 and bimetallic Pd-Fe/SiO_2 catalysts. The most important result on Pd-Fe bimetallic catalyst is the formation of 2-methylfuran which can be derived from the C—O hydrogenolysis of furfuryl alcohol. As shown in Table 2 (entry 5), when feeding furfuryl alcohol there is no significant amount of 2-methyfuran formed on Pd/SiO_2 (yield < 1%). It is also interesting to note that the major product from furfuryl alcohol on 1%Pd/SiO_2 is a saturation of furanyl ring to tetrahydro furfuryl alcohol. In contrast, more than 83% of furfuryl alcohol is converted to 2-methylfuran with 1%Pd-0.5%Fe/SiO_2 catalyst. The results from this work have demonstrated that bimetallic Pd-Fe catalyst is very selective toward C—O bond cleavage reactions instead of C—C bonds which mainly occur on monometallic Pd catalyst.

Table 2
Conversion and yield of products from the reaction of furfural and furfuryl alcohol over 1%Pd/SiO_2 and 1%Pd-0.5%Fe/SiO_2 catalysts in vapor phase.

Entry	Catalysts	Feed	Conv. (%)	Yield (%)					Selectivity (%)	
				Furan	THF	FOL	MF	HFOL	DeCO[b]	HyCO[c]
1	Pd/SiO_2	FAL	82.1	54	13.4	11	0	3.8	82.1	18.0
2	Pd-Fe/SiO_2	FAL	81.4	13.5	0.0	19.0	38.6	10.2	16.6	83.3
3	[a]Pd/SiO_2 + Fe/SiO_2	FAL	80.3	53	11.9	10.6	0.1	4.8	80.8	19.3
4	Fe/SiO_2	FAL	0.0	0.0	0.0	0.0	0.0	0.0	–	–
5	Pd/SiO_2	FOL	19.2	2.0	2.8	–	0.7	13.7	–	–
6	Pd-Fe/SiO_2	FOL	92.7	2.8	0.4	–	83.3	6.2	–	–
7	[a]Pd/SiO_2 + Fe/SiO_2	FOL	19.6	1.6	2.0	–	1.0	15.1	–	–
8	Fe/SiO_2	FOL	0.0	0	0	–	0	0	–	–

Reaction conditions: Temp. = 250 °C, H_2/Feed molar ratio = 25, pressure = 1 atm, W/F = 0.075 h.
[a] Physical mixture of two catalysts.
[b] DeCO = decarbonylation (see Scheme 1) DeCO products = Furan + THF.
[c] HyCO = hydrogenation (see Scheme 1) HyCO products = FOL + MF + HFOL.

3.2.2. Effect of support on the 2-methylfuran selectivity

To explore the effect of the support on the gas phase furfural conversion, a bimetallic Pd-Fe supported over γ-Al_2O_3 was evaluated. The results are shown in Fig. 7.

A significant difference with the product distribution from Pd-Fe/SiO_2 is observed. First, the yield of 2-methylfuran was much lower than over the SiO_2-supported bimetallic. In this case, the C—C scission is the preferred pathway displaying a high yield of furan, similar to that of pure Pd. As a result, the selectivity to MF is dramatically lower than on SiO_2 and similar to that of Pd/SiO_2, as illustrated in Fig. 8.

As it was expected, with the Pd-Fe/SiO_2 catalyst the selectivity toward 2-methylfuran increases with the furfural conversion, while with Pd/SiO_2 catalyst there was not selectivity since there was no formation of 2-methylfuran. The product selectivity was drastically shifted to furan when Pd-Fe nanoparticles were supported on γ-Al_2O_3. This could be due to the higher interaction of the metallic nanoparticles with the γ-Al_2O_3 support, which caused the two-metal segregation as shown in the XPS, XRD and TEM analysis. In this way, Pd-Fe/γ-Al_2O_3 catalyst behaves a lot more like monometallic Pd/SiO_2. Since the physical mixture of Pd/SiO_2 and

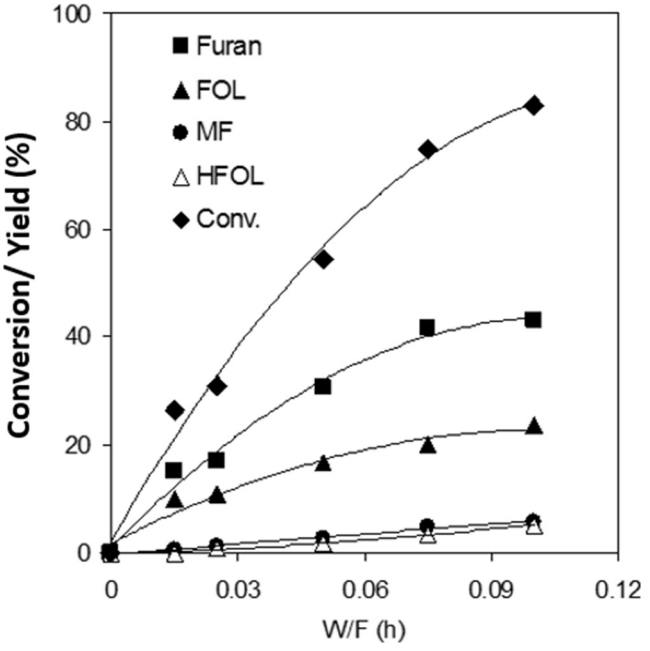

Fig. 7. Product distribution from the reaction of furfural over a bimetallic 1%Pd-0.5%Fe/g-Al_2O_3 catalyst, at 250 °C, H_2/Feed molar ratio = 25, pressure = 1 atm. FOL = furfuryl alcohol, MF = 2-methylfuran, HFOL = tetrahydrofurfuryl alcohol.

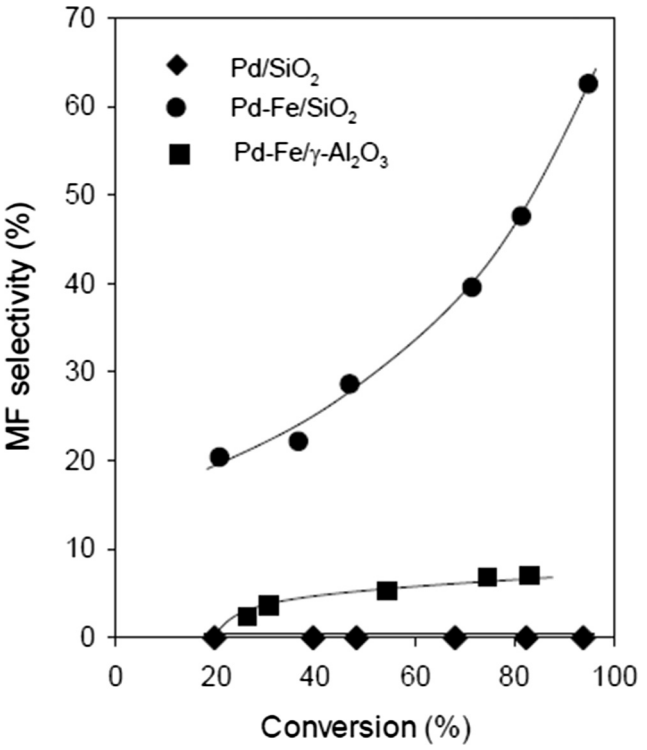

Fig. 8. 2-Methylfuran selectivity as a function of furfural conversion over supported Pd-Fe catalysts at 250 °C, H_2/Feed molar ratio = 25, pressure = 1 atm.

Fe/SiO_2 showed a low yield of 2-methylfuran (Table 2), one could expect the formation of Pd-Fe bimetallic alloy, which is required for the C—O hydrogenolysis may not be totally formed on γ-alumina support; therefore, nanoparticles of Pd and Fe behave individually.

Fig. 8 shows the yield and selectivity to 2-methylfuran (MF) over the Pd-Fe/SiO_2 and Pd-Fe/γ-Al_2O_3 catalysts. It is clear that, at the same furfural conversion (~80%) the selectivity to 2-methylfuran over the Pd-Fe/SiO_2 catalyst was much higher (46.3%) than that over Pd-Fe/γ-Al_2O_3 (only 8.5%). The high selectivity toward 2-methylfuran on the silica supported catalyst is a clear indication of the Pd-Fe alloy formation, which is not present when alumina was used as support.

3.2.3. Reaction in liquid phase

The product distribution obtained from furfural conversion in liquid phase (decalin solvent) was investigated on the same catalyst series used in the vapor phase. It was found that the main

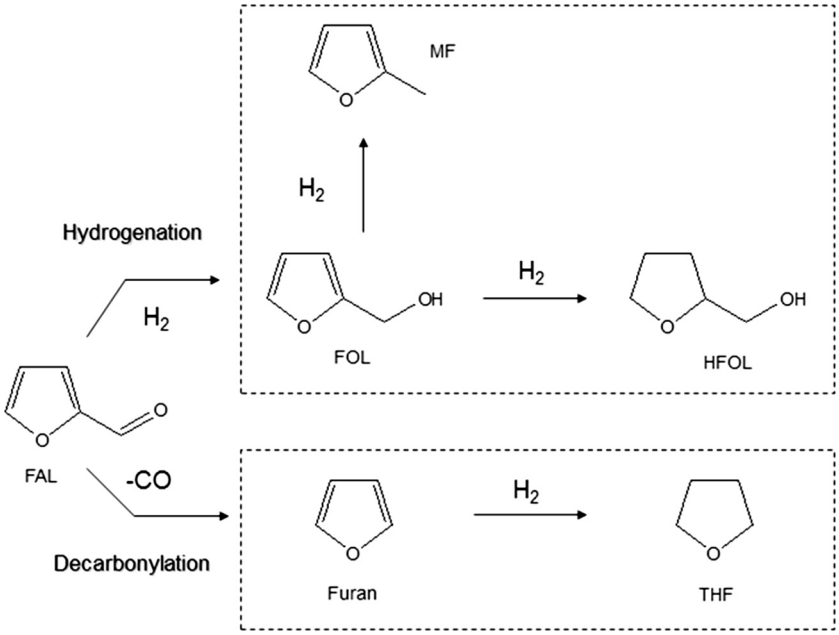

Scheme 1. Reaction pathways for furfural conversion.

product from the liquid phase reaction of furfural on 1%Pd/SiO_2 at 250 °C was furan. Hydrogenation products, such as tetrahydrofuran, obtained from secondary furan hydrogenation, and furfuryl alcohol, from primary furfural hydrogenation (see Scheme 1) were also observed, but at lower yields than that of furan. This means that decarbonylation is the preferred reaction pathway for the conversion of furfural over pure Pd. Even at high furfural conversion, no formation of 2-methylfuran was observed over Pd/SiO_2. Similar results have been found by Bhogeswararao et al. [6], who obtained high furan yield (82%) and selectivity using supported Pd catalysts in liquid phase (isopropanol solvent). Likewise, Wang et al. [47] achieved high selectivity to furan (98%) in a reaction of furfural over a core-shell structural Pd@S-1 catalyst, using butanol as a solvent.

By contrast, over the 1%Pd-0.5%Fe/SiO_2 catalyst, 2-methylfuran and furfuryl alcohol were the main reaction products (see Table 3 and Scheme 1). In the batch reactor, at increasing reaction times the yield of furfuryl alcohol decreased as the yield of 2-methylfuran increased. Similar behavior was observed by Scholz et al. [48], who investigated the liquid phase conversion of furfural over Pd catalysts. They found that the formation of 2-methylfuran greatly increased when Pd was supported on Fe_2O_3 compared to other supports. The same trend has been reported for other bimetallic catalysts in the liquid phase, including Cu-Co and Cu-Fe at varying molar ratios [13,15,49].

Table 3 shows that hydrogenation of furan to tetrahydrofuran also occurred over 1%Pd-0.5%Fe/SiO_2, but with a significantly lower yield than over Pd/SiO_2. Interestingly, when γ-Al_2O_3 was used as a support in the liquid phase, the unbalance carbon greatly increased, leading to lower yields of 2-methylfuran and furfuryl alcohol. This loss in carbon yield may be associated with the acidity of γ-Al_2O_3, which promotes oligomerization, coke formation, and consequently, catalyst deactivation. Hydrogenation of 2-methylfuran to 2-methyltetrahydrofuran was also observed on this catalyst.

Another interesting by-product, observed over Pd-Fe/SiO_2 and Pd-Fe/γ-Al_2O_3 catalysts in liquid phase but not in vapor phase, was cyclopentanone. This C—C bond forming product has been previously observed in furfural reactions and is ascribed to the Piancatelli rearrangement of furfuryl alcohol, favored by the presence of water [50–52], which is produced in the C—O hydrogenolysis of furfuryl alcohol to 2-methylfuran.

The major differences between the results in gas and liquid phase can be summarized as follows. Over Pd/SiO_2 the product distribution obtained at the same overall conversion was very similar, regardless of whether the reaction was conducted in vapor or liquid phase. Over Pd-Fe/SiO_2, the major difference was the almost complete disappearance of furan in the products when the reaction was conducted in the liquid phase. That is, the effect of the alloy, which causes a great decrease in decarbonylation rate in the vapor phase is further enhanced in the presence of the solvent, since decarbonylation requires an ensemble of Pd sites with strong bond to the adsorbate and the addition of Fe suppresses this activity. Similar conclusions have been recently derived by Yang et al. [53] in their study of furfural and methyl-isobutylketone conversion on Pd-FeO_x/SiO_2 catalysts. Working under solvent-free hydrodeoxygenation conditions, they found that relative to monometallic Pd, the Pd-Fe catalyst gave less decarbonylation products. They explained this behavior in terms of Pd ensemble dilution on the basis of experimentally demonstrated (EXAFS, Mossbauer) decrease in Pd-Pd coordination number by addition of Fe, which inhibits C—C bond breaking by decarbonylation. Our results further suggest that the solvent may further enhance the site blockage, thus reducing the production of furan. Interestingly, the production of MF via C—O bond hydrogenolysis, enhanced by alloying with Fe, is not greatly affected by the presence of the solvent.

3.3. DFT calculations on Pd(1 1 1), Pd_3Fe_1(1 1 1) and Pd_2Fe_2(1 1 1) surfaces

DFT calculations were conducted to interpret the changes observed in product selectivity on Pd-Fe bimetallic catalysts compared to the monometallic Pd catalyst. Two aspects should be explored; first, the addition of Fe causes a decrease in the C—C bond cleavage reaction [7], but also it causes an increase in the HDO reaction, in good agreement with the results reported by

Table 3
Conversion and yield of products from the reaction of furfural over Pd and Pd-Fe catalysts in vapor and liquid phase.[a]

	Product yield (%)					
	Pd/SiO_2		$Pd\text{-}Fe/SiO_2$		$Pd\text{-}Fe/\gamma\text{-}Al_2O_3$	
	Vapor	Liquid phase	Vapor	Liquid phase	Vapor	Liquid phase
Conversion (%)	68	68	82	84	80	89
Furan	47	36	13	0.13	40	6
FOL	10	7	20	21	21	7
THF	11	13	0	7	0	0
MF	0	0	40	36	10	20
HFOL	0.3	0	9	0	9	0
MTHF	0	0	0	0	0	14
CPON	0	0	0	2	0	9
Unbalance carbon (%)	0	12	0	18	0	33

[a] FOL = furfuryl alcohol, THF = tetrahydrofuran, MF = 2-methylfuran, THFOL = tetrahydrofurfuryl alcohol, MTHF = 2-methyltetrahydrofuran, CPON = cyclopentanone.

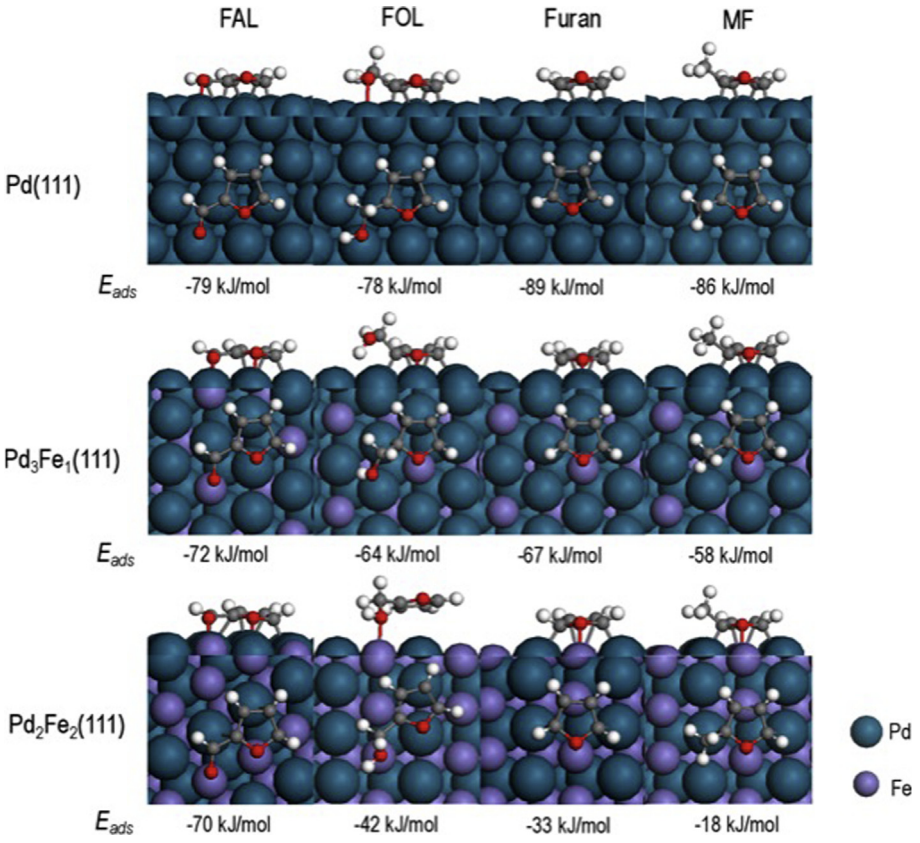

Fig. 9. DFT optimized adsorption structures of furfural, furfuryl alcohol and furan on Pd(111), $Pd_3Fe_1(111)$ and $Pd_2Fe_2(111)$ surfaces and the corresponding adsorption energies.

Wang et al. on the conversion of phenolic compounds such as cresol [54] and guaiacol [55] over bimetallic Pd-Fe catalysts.

To investigate the interaction of furanic compounds with the monometallic and bimetallic surfaces, we conducted DFT calculations to obtain adsorption energies of furfural, furfuryl alcohol, furan and methylfuran on optimized structures of Pd(111), $Pd_3Fe_1(111)$ and $Pd_2Fe_2(111)$.

The possible adsorption modes of these furanics on different metal surfaces were shown in the supporting information Fig. S6, and the most favorable adsorption structures and the corresponding adsorption energies are shown in Fig. 9. On Pd(111), all these four furanics favorably adsorb via the furanic ring with the adsorption energy around −79 to −89 kJ/mol. The addition of Fe weakens the adsorption of furanic ring. Therefore, the adsorption energies of all the four furanics decrease along with the content of Fe. That is, on $Pd_3Fe_1(111)$, the adsorption energies of furan, methylfuran and furfuryl alcohol decrease to −67 kJ/mol, −58 kJ/mol and −64 kJ/mol respectively. On $Pd_2Fe_2(111)$, they further decrease to −33 kJ/mol, −18 kJ/mol and −42 kJ/mol, respectively. The furanic ring adsorption on $Pd_2Fe_2(111)$ is so weak that it is more favorable for furfuryl alcohol to adsorb via the —OH side group rather than the furanic ring, as shown in Fig. 9. The weaker binding of the furanic ring on the Pd-Fe alloy surface is probably due to both the electronic effects and the ensemble effects. The *d* band center of $Pd_3Fe_1(111)$ and $Pd_2Fe_2(111)$ was calculated to be −1.66 eV and −1.70 eV respectively, which are lower than the monometallic Pd (111) surface (−1.46 eV). As the d-band shifts up in energy, the number of antibonding states above ε_F (Fermi level) increases,

which leads to a stronger bond, as clearly occurring with Pd(1 1 1) surface. Furthermore, according to the literature, lower d band center leads to weaker binding of species [56].

The weak binding of the furan ring on Pd-Fe alloy surface compared to the monometallic Pd(1 1 1) surface leads to the increased difficulty in ring hydrogenation, which is consistent with the experimental observation that much less ring hydrogenation products (THF, MTHF) were observed over Pd-Fe/SiO_2 than over Pd/SiO_2.

Unlike furan, methylfuran or furfuryl alcohol, the adsorption of furfural on Pd_3Fe_1(1 1 1) and Pd_2Fe_2(1 1 1) does not change much relative to adsorption on Pd(1 1 1). This is clearly due to the stronger bond of the carbonyl group to the oxophilic Fe atoms, as illustrated in Fig. 9. This is further confirmed by our calculations of the adsorption of formaldehyde (H_2C═O) on Pd(1 1 1), Pd_3Fe_1(1 1 1) and Pd_2Fe_2(1 1 1) via only the carbonyl group. Indeed, they showed stronger adsorption on Pd_3Fe_1(1 1 1) (−92 kJ/mol) and Pd_2Fe_2(1 1 1) (−85 kJ/mol) rather than on Pd(1 1 1) (−55 kJ/mol). Similarly, the stronger adsorption of the side group —OH of furfuryl alcohol on Pd-Fe alloy surface than the monometallic Pd(1 1 1) surface was shown by the adsorption energies of CH_3OH on Pd_3Fe_1(1 1 1) (−46 kJ/mol), Pd_2Fe_2(1 1 1) (−42 kJ/mol) and Pd(1 1 1) (−26 kJ/mol), as shown in Fig. S7.

These results clearly explain the great differences in selectivity between Pd and Pd-Fe alloys, with the former preferring C—C bond cleavage via decarbonylation and the latter C—O bond cleavage via hydrogenolysis. The weaker binding of the furanic ring but stronger binding of the carbonyl group and —OH group on Pd-Fe alloy surface than Pd(1 1 1) leads to enhanced HDO activity. At the same time, the stronger binding of the carbonyl group on Pd-Fe alloy surface facilitates hydrogenation of furfural to furfuryl alcohol and further deoxygenation to methylfuran. By contrast, the decarbonylation of furfural requires the adsorption of the furanic ring after the C—C bond breaking, which is expected to be difficult due to the unfavorable binding of furanic ring on the Pd-Fe alloy surface, as shown above. This is in good agreement with the experiments over Pd-Fe alloys that show lower selectivity to furan with enhanced selectivity to furfuryl alcohol and methylfuran. The opposite is true on pure Pd or bimetallic catalysts in which the alloying of Pd and Fe is prevented by the interaction with the support (e.g. alumina).

4. Conclusion

The gas phase conversion of furfural over bimetallic Pd-Fe/SiO_2 catalyst gives predominantly 2-methylfuran, while over monometallic Pd/SiO_2 catalyst, the decarbonylation reaction dominates, yielding furan as the main product. This means that an alloying metal like Fe with a strong affinity for oxygen enhances the selectivity toward C—O hydrogenolysis, forming 2-methylfuran as a final product.

The change of the support affects the formation of Pd-Fe alloy and consequently the selectivity toward 2-methylfuran. When using γ-Al_2O_3 instead of SiO_2 as a support of the bimetallic catalyst, the selectivity greatly changes from 2-methylfuran to furan. That is, Pd-Fe/γ-Al_2O_3 behaves much more like a monometallic Pd/SiO_2 than a bimetallic Pd-Fe/SiO_2. These results suggest that the intrinsic properties of support have significant influence on the catalytic performance of Pd-Fe catalysts. The observed contrasting behavior of the two supports is explained in terms of a segregation of the metals induced by a higher interaction with the support, in the case of alumina that does not occur on silica, as evidenced by XPS, XRD, and TEM characterization.

The presence of the solvent enhances the inhibition of the decarbonylation path via acyl intermediate. As a result, in the liquid phase the maximum methylfuran/furan product ratio is obtained. However, carbon losses and catalyst deactivation are much higher in the liquid phase compared to gas phase operation.

DFT calculations show that furfural, furfuryl alcohol, furan and methylfuran favorably adsorb via the furanic ring on Pd(1 1 1), while the addition of Fe clearly weakens these adsorption energies. The stronger binding of the carbonyl group (strongly bound to the oxophilic Fe) and —OH group on Pd-Fe alloy surface promotes the furfural hydrogenation and furfuryl alcohol hydrogenolysis toward 2-methylfuran.

Acknowledgments

This work was supported by the Department of Energy, with funding of the experimental part under grant DE-SC0004600 (DoE-EPSCOR) and theoretical part under grant DE-EE0006287 (BETO/CHASE program). NP gratefully acknowledges the Universidad de Antioquia (Colombia) for a scholarship and COLCIENCIAS (Colombia) for financial support (1115-569-33557).

Appendix A. Supplementary material

Supplementary data associated with this article can be found, in the online version, at http://dx.doi.org/10.1016/j.jcat.2017.03.016.

References

[1] R. Mariscal, P. Maireles-Torres, M. Ojeda, I. Sádaba, M. López Granados, Energy Environ. Sci. 9 (2016) 1144–1189.
[2] D.E. Resasco, S. Sitthisa, J. Faria, T. Prasomsri, M.P. Ruiz, in: D. Kubicka, I. Kubicková (Eds.), "Heterogeneous Catalysis in Biomass to Chemicals and Fuels" Research Signpost, 2012, pp. 155–188.
[3] A. Mandalika, T. Runge, Green Chem. 14 (2012).
[4] T.N. Pham, D. Shi, D.E. Resasco, Appl. Catal. B Environ. 145 (2014) 10–23.
[5] Y. Roman-Leshkov, C.J. Barrett, Z.Y. Liu, J.A. Dumesic, Nat. Lett. 447 (2007) 982.
[6] S. Bhogeswararao, D. Srinivas, J. Catal. 327 (2015) 65–77.
[7] S. Sitthisa, W. An, D.E. Resasco, J. Catal. 284 (2011) 90–101.
[8] H.-Y. Zheng, Y.-L. Zhu, B.-T. Teng, Z.-Q. Bai, C.-H. Zhang, H.-W. Xiang, Y.-W. Li, J. Mol. Catal. A Chem. 246 (2006) 18–23.
[9] B.-M. Nagaraja, A.-H. Padmasri, B. Raju, K.-S. Rama, J. Mol. Catal. A: Chem. 265 (2007) 90–97.
[10] M.-M. Villaverde, N.-M. Bertero, T.-F. Garetto, A.-J. Marchi, Catal. Today 213 (2013) 87–92.
[11] C.-P. Jiménez, J.-A. Cecilia, I. Márquez, R. Moreno, J. Santamaría, J. Mérida, P. Maireles, Catal. Today 279 (2017) 327–338.
[12] L. Liu, H. Lou, M. Chen, Int. J. Hydrogen Energy (2016).
[13] H. Sheng, R.-F. Lobo, ChemCatChem. 8 (2016) 1–8.
[14] K. Yan, A. Chen, Fuel 115 (2014) 101–108.
[15] X. Chang, A.-F. Liu, B. Cai, J.-Y. Luo, H. Pan, Y.-B. Huang, ChemSusChem. 9 (2016) 1–9.
[16] K. Xiong, W. Wan, J. Chen. Surf. Sci. 652 (2016) 91–97.
[17] W.T. Yu, M.D. Porosoff, J.G. Chen, Chem. Rev. 112 (2012) 5780.
[18] S. Sitthisa, T. Pham, T. Prasomsri, T. Sooknoi, R. Mallinson, D.E. Resasco, J. Catal. 280 (2011) 17–27.
[19] W. Yu, K. Xiong, N. Ji, M.D. Porosoff, J.-G. Chen, J. Catal. 317 (2014) 253–262.
[20] M. Hansen, Constitution of Binary Alloys, McGraw-Hill, New York, 1958, p. 696.
[21] G. Willimas, J.W. Loram, J. Phys. Chem. Solids 30 (1969) 1827–1833.
[22] R. Madon, M. Boudart, Ind. Eng. Chem. Fundament. 21 (1982) 438–447.
[23] G. Kresse, J. Hafner, Phys. Rev. B 47 (1993) 558–561.
[24] J.P. Perdew, K. Burke, M. Ernzerhof, Phys. Rev. Lett. 77 (1996) 3865–3868.
[25] G. Kresse, D. Joubert, Phys. Rev. B 59 (1999) 1758–1775.
[26] G. Ghosh, C. Kantner, G.B. Olson, J. Phase Equilib. 20 (1998) 295–310.
[27] G.L.W. Hart, S. Curtarolo, T.B. Massalski, O. Levy, Phys. Rev. X 3 (2013), 041035-1–041035-33.
[28] R.V. Chepulskii, S.V. Barabesh, A. Zunger, Phys. Rev. B 85 (2012), 144201-1–144201-23.
[29] Y. Chen, T. Atago, T. Mohri, J. Phys.: Condens. Matter 14 (2002) 1903–1913.
[30] K.H.J. Buschow, P.G. van Engen, R. Jongebreur, J. Magn. Magn. Mater. 38 (1983) 1–22.
[31] W. Olovsson, T. Marten, E. Holmstrom, B. Johansson, I. Abrikosov, J. Electron. Spectrosc. Relat. Phenom. 178 (2010) 88–99.
[32] Q.T. Trinh, K.F. Tan, A. Borgna, M. Saeys, J. Phys. Chem. C 117 (2013) 1684–1691.
[33] F. Pinna, M. Selva, M. Signoretto, G. Strukul, F. Boccuzzi, A. Benedetti, P. Canton, G. Fagherazzi, J. Catal. 150 (1994) 356–367.
[34] Y. Tang, S. Cao, Y. Chen, T. Lu, Y. Zhou, L. Lu, Bao, J. Appl. Surf. Sci. 256 (2010) 4196–4200.

[35] S.N. Babu, N. Lingaiah, J.V. Kumar, P.S.S. Prasad, Appl. Catal. A Gen. 367 (2009) 70–76.
[36] B.L. Gustafson, P.S. Wehner, Appl. Surf. Sci. 52 (1991) 261–270.
[37] K. McEleney, C.M. Crudden, J.H. Horton, J. Phys. Chem. C 113 (5) (2009) 1901–1907.
[38] J. Tarabay, W. Al-Maksoud, F. Jaber, C. Pinel, S. Prakash, L. Djakovitch, Appl. Catal. A Gen. 388 (2010) 124–133.
[39] M.P. Felicissimo, O.N. Martyanov, T. Risse, H.J. Freund, Surf. Sci. 601 (2007) 2105–2116.
[40] J.C. Bertolini, J.L. Rousset, P. Miegge, J. Massardier, B. Tardy, Surf. Sci. 287 (288) (1993) 346.
[41] S.L. Zhang, J.R. Zhang, Phys. Stat. Sol. B 182 (1994) 421.
[42] G.M. Nunez, A.J. Rouco, J. Catal. 111 (1988) 41–49.
[43] S. Sitthisa, D.E. Resasco, Catal. Lett. 141 (2011) 784–791.
[44] R.D. Srivastava, A.K. Guha, J. Catal. 91 (1985) 254–262.
[45] S. Sitthisa, T. Sooknoi, Y.G. Ma, P.B. Balbuena, D.E. Resasco, J. Catal. 277 (2011) 1–13.
[46] J.A. Cecilia, D. Duran-Martin, R. Moreno-Tost, Ramon, J. Santamaria-Gonzalez, J. Catal. 336 (2016) 107–115.
[47] C. Wang, L. Wang, J. Zhang, H. Wang, J.-P. Lewis, F.–Sh. Xao, J. Am. Chem. Soc. 138 (2016) 7880–7883.
[48] D. Scholz, Ch. Aellig, I. Hermans, ChemPubSoc. 7 (2014) 268–275.
[49] S. Srivastava, G.-C. Jadeja, J. Parikh, RSC Adv. 6 (2016) 1649–1658.
[50] G. Piancatelli, A. Scettri, S. Barbadoro, Tetrahedron Lett. 17 (1976) 3555–3558.
[51] K. Fulajtarova, T. Sotak, M. Hronec, I. Vavra, E. Dobrocka, M. Omastova, Appl. Catal. A 502 (2015) 78–85.
[52] T.V. Bui, S. Crossley, D.E. Resasco, in: Cavani et al. (Eds.), Chemicals and Fuels from Bio-Based Building Blocks, 2016 (Chapter 17).
[53] J.F. Yang, S.S. Li, L.L. Zhang, X.Y. Liu, J.H. Wang, X.L. Pan, N. Li, A.Q. Wang, Y. Cong, X.D. Wang, T. Zhang, Appl. Catal. B – Environ. 201 (2017) 266–277.
[54] Y. Hong, H. Zhang, J. Sun, A.M. Karim, A. Hensley, M. Gu, M.H. Engelhard, J.S. McEwen, Y. Wang, ACS Catal. 4 (2014) 3335–3345.
[55] J. Sun, A.M. Karim, H. Zhang, L. Kovarik, X.S. Li, A. Hensley, J.S. McEwen, Y. Wang, J. Catal. 306 (2013) 47–57.
[56] J.-K. Norskov, F.-A. Pedersen, F. Studt, T. Bligaard, PNAS 108 (2011) 937–943.